Structural insight in TiO_2 supported CoFe catalysts for Fischer -Tropsch synthesis at ambient pressure

M. Russo[1], V. La Parola[1*], G. Pantaleo[1], M. L. Testa[1], A.M. Venezia[1•]

R. Gupta[2], A. Bordoloi[2], R. Bal[2]

[1] *ISMN-CNR, Via Ugo La Malfa 153, 90146 Palermo, Italy*

[2] *Indian Institute of Petroleum, Dehradun, Uttaranchal, India*

Monometallic and bimetallic iron cobalt catalysts supported on home- made TiO_2 were prepared by microwave assisted co-precipitation. The obtained samples, containing a total metal loading of 12 wt%, in different Co/Fe weight ratios, were characterized by N_2-adsorption-desorption isotherms, XRD, H_2-TPR, XPS and HRTEM techniques. The catalysts were tested in Fischer-Tropsch Synthesis reaction under atmospheric pressure using a continuous flow reactor with a gas feed of CO and H_2 in He (CO:H_2:He volume ratio of 1:1.7:2.3). The molar ratio H_2/CO was set to 1.7:1, slightly lower with respect to the stoichiometric value of 2. The experiments were performed in the temperature range of 250 - 350 °C. Significant amount of methane and C_2-C_4 hydrocarbons formed at low temperature with all the catalysts. The selectivity to higher hydrocarbon increased with temperature. The iron containing catalysts gave rise to CO_2 and also to methanol. The bimetallic catalysts exhibited the best performance in terms of CO conversion and selectivity to C_2-C_4 and high C_{5+} hydrocarbons. Co_xFe_y crystallites, detected by XRD, represented part of the active sites, contributing to the catalytic activity. The observed structural transformation of the samples during the H_2 pre-treatment and during the catalytic reaction were related to the catalytic behavior of these catalytic materials.

Keywords: Fischer- Tropsch synthesis, ambient pressure, TiO_2 support, Cobalt Iron catalysts, Co_xFe_y
alloys.

• Corresponding author: E-mail address: annamaria.venezia@cnr.it; valeria.laparola@cnr.it

Introduction.

The environmental impact of CO_2 emissions, associated to the observed climate change, relates to the extensive consumption of fossil fuels as energy source for stationary and for transportation purposes [1]. Additionally, conventional reserves of fossil fuels are continuously depleting [2]. The combination of these two aspects with an increase global demand for fuel supplies has given a renewed impetus to the exploitation of the Fischer-Tropsch Synthesis (FTS) technology. The FTS process consists in a catalyzed polymerization reaction, starting from synthesis gas, a mixture of H_2 and CO, obtained from natural gas or coal gasification, leading to the formation of hydrocarbons of different chain length and water [3]. In order to comply with increasing regulations on CO_2 emission, the biomass to liquid (BTL) technology, based on Fischer-Tropsch synthesis, with syngas derived from biomass, may play an important role in a sustainable economy, being almost CO_2 neutral [4]. The obtained fuels are high quality diesel characterized by high cetane number and low content of sulfur and aromatics. However, the cost of running the FTS plants is still quite expensive as compared to the direct production of gasoline or diesel from crude oil. Indeed, current commercial FT processes operate at high pressures of 20-40 bar, raising safety concerns [5]. The main reactions occurring during the FTS process are the following:

$$(2n+1)H_2 + nCO \rightarrow C_nH_{2n+2} + nH_2O \quad (1)$$

$$2nH_2 + nCO \rightarrow -CH_2- + H_2O \quad (2)$$

$$CO+H_2O \rightarrow CO_2 + H_2 \quad (3)$$

$$2nH_2 + nCO \rightarrow C_nH_{2n+2}O + (n-1)H_2O \quad (4)$$

$$2CO \rightarrow C + CO_2 \quad (5)$$

All the processes, with the exception of (5) are highly exothermic. Equations 1 and 2 lead to generation of alkanes and alkenes respectively, whereas equation 3, corresponding to the water gas shift reaction (WGS), provides a way to adjust the molar H_2/CO ratio. Side reactions producing alcohols and undesired carbonaceous deposits through the Boudouard reaction may occur respectively through equation 4 and equation 5 [6]. The accepted mechanism for the FT synthesis involves first the dissociative adsorption of CO and H_2. Then, the formed carbide species, reacting with the adsorbed dissociated hydrogen, generates the CH_2-intermediates giving rise to the propagation step and chain growth termination. It is therefore understandable how an appropriate catalyst design in terms of chemical formulation, morphology and structural properties would contribute to optimize the selectivity of the FTS towards valuable C_{5+} products. In fact, the research on improvement of catalysts to increase the conversion rate and the selectivity to the desired hydrocarbons is still a challenging task [7]. Fe, Co, Ni, Ru are the most active metals for the FTS process. Ru is rather expensive and therefore is not suitable for industrial application. Nickel,

having a high hydrogenation activity, has a tendency to form methane. Cobalt and iron are the metals of choice for large-scale FTS processes [8, 9]. Cobalt has a high activity at lower temperature (200 - 250 °C), a good selectivity to linear C_{5+} hydrocarbons and is more resistant to deactivation. Iron is economically attractive, being cheaper than cobalt. It generally operates at high temperature (300 – 350 °C) and has a good selectivity to olefins, however, it deactivates quickly. Whereas for the cobalt catalysts it is widely accepted that the active sites for the initiation of the FTS process are represented by Co sites, relatively to the iron catalysts, the identification of the active sites is rather debatable [10]. Some researchers claim that the active species is the Fe_3O_4, while others claim that the active species is an iron carbide or even a mixture of the two phases plus metallic iron [9-11]. The catalyst support plays also an important role on the reducibility and surface dispersion of the active metal species. Generally, a support like Al_2O_3, strongly interacting with the metal oxide, increases the cobalt dispersion while decreasing its reducibility. Opposite is the case of a silica carrier that, by weakly interacting with cobalt, would favor the reducibility but at the expenses of the catalyst dispersion [4]. Several studies reported TiO_2 as a suitable support for cobalt catalysts since it grants a good balance between reducibility and metal dispersion [11-16]. Beside the intrinsic nature of the metals, the H_2/CO ratio of the feed, dictates the choice between cobalt- or iron- based catalysts. In the gas-to-liquid (GTL) technology, where the syngas is obtained from natural gas with ratio $H_2/CO \geq 2$, cobalt catalysts are typically used [6]. For BTL technology, where the used bio-syngas has a molar ratio below 2, the presence of iron, characterized by a high WGS activity, would enhance the FTS activity and increase the selectivity to the C_{5+} hydrocarbons [17-18]. Co and Fe are often combined together in order to decrease the high cost of the cobalt catalysts, still maintaining good catalytic performance [4, 16]. For an upcoming application of the FT process, coupled with small anaerobic digestion plants for the generation of syngas, it would be particularly desirable to operate the FT at ambient pressure, decreasing the risk related to high pressure plants and also decreasing the complexity of the all apparatus [5].

The objective of the present study, in this context, is the development of TiO_2 supported Co-Fe catalysts with good efficiency and selectivity in FTS reaction. In particular, mono metallic and bimetallic catalysts with different Co/Fe ratio are considered. Ambient pressure condition of the catalytic reaction is chosen to test the low pressure conditions as a viable solution for a more sustainable FT process [5]. Moreover, in such condition the catalyst surface would not be extensively covered with carbonaceous products, allowing for an easier characterization of the catalyst surface. The results are discussed in terms of structural, morphological and electronic properties of the different systems, as obtained by a variety of characterization techniques.

2. Experimental

2.1 Support and catalyst preparation

The TiO_2 support was prepared by a sol-gel procedure in the presence of triblock polymer, Pluronic P123 [19]. The mixture of the polymer dissolved in 2-propanol, containing HCl diluted in water, was stirred overnight at 35 °C in a 250 mL one neck flask. $Ti(i\text{-}PrO)_4$ was quickly added to this solution (final molar composition as 1.0 $Ti(i\text{-}PrO)_4$: 34 C_3H_7O: 0.04 HCl: 3 H_2O: 0.02 P-123) and stirred for 24 h at the same temperature. Then, the milky suspension was aged at 100 °C for 24 h in a closed polypropylene bottle. The solid product was filtered, washed with EtOH and calcined in air at 500 °C for 5 h (heating rate of 2 °C/min). Mono (Fe, Co) and bimetallic (FeCo) catalysts were prepared by co-precipitation assisted by microwave [20]. Namely, an aqueous solution of iron and/or cobalt nitrate (20 ml) was added to a suspension of the home made TiO_2 in ethanol (40 ml). The metal hydroxides were precipitated by adding dropwise NH_4OH until pH = 9. The obtained slurry was placed inside a conventional household microwave set at a power of 180 Watts and operated in 30 s cycles (on for 10 s and off for 20 s) for a total irradiation time of 10 min. The collected precipitate, washed with distilled water and ethanol, was dried at 100 °C for 1 h and then calcined at 500 °C for 2 h. Catalysts are labeled as $12Fe/TiO_2$, $12Co/TiO_2$, $6Co6Fe/TiO_2$ and $10Co2Fe/TiO_2$, with the digits representing the supported element wt%. The given composition in terms of Fe and Co content was confirmed by Atomic Emission Spectroscopy (MP-AES 4200 Agilent technologies).

2.2 Catalyst characterization

Specific surface areas and pore volumes were determined from N_2 adsorption –desorption isotherms at -196 °C using a Micromeritics ASAP 2020 equipment, through the Brunauer –Emmett-Teller (BET) method in the standard pressure range 0.05–0.3 P/P^0. Before the measurements, the samples were degassed at 250 °C for 2h. By analysis of the desorption curve, using the BJH calculation method, the pore size distribution was also obtained. The total pore volume (V_p) was evaluated on the basis of the amount of nitrogen adsorbed at a relative pressure of about 0.98.

X-ray diffraction (XRD) analyses were performed with a Bruker goniometer using Ni-filtered Cu Kα radiation. A proportional counter and 0.05° step size in 2θ were used. The assignment of the crystalline phases was based on the JPDS powder diffraction file cards [21]. Crystallite sizes were estimated from diffraction line widths using the Sherrer equation [22].

The X-ray photoelectron spectroscopy (XPS) analyses were performed with a VG Microtech ESCA 3000 Multilab, equipped with a dual Mg/Al anode. As excitation source was used the Al Kα radiation (1486.6 eV). The sample powders were mounted on a double-sided adhesive tape. The pressure in the analysis chamber was in the range of 10^{-8} Torr during data collection. Contact of the spent catalysts with air was minimized by keeping them under inert gas until being transferred

through a glove box into the XPS instrument. In selected cases, spectra were recorded also on reduced samples. The reduction was carried out inside a high pressure chamber, directly connected to the analysis chamber, under H_2 flow at 350 °C for 16 h, i.e., under the same experimental conditions as those used for the pretreatment prior to catalytic test. All the energies were referred to the C 1s binding energy set at 285.1 eV arisen from adventitious carbon. The reliability of the calibrated binding energies was also confirmed with respect to the Ti $2p_{3/2}$ binding energy taken as internal reference, calibrated for the pure TiO_2 support at 358.8 eV. Analyses of the peaks were performed with the CasaXPS software. Atomic concentrations were calculated from peak intensity using the sensitivity factors provided by the software. The binding energy values were quoted with a precision of ± 0.15 eV and the atomic percentage with a precision of ± 10%.

Hydrogen temperature programmed reduction (TPR) measurements were carried out with a Micromeritics AutoChem 2950HP Automated Catalyst Characterization System, equipped with a thermal conductivity detector (TCD). About 0.1 g of sample was used for each measurement. The samples were pre-treated with a mixture of 5 vol % O_2 / He at 50 ml/min, heating up (10 °C/min) to 400 °C and holding at this temperature for 30 min. After lowering the temperature down to room temperature, the gas mixture of 5 vol % H_2 / Ar was introduced at 30 ml/min into the sample tube and was also used as a reference gas. During the analysis, the temperature was increased up to 1000 °C at a rate of 10 °C/min. The effluent gas was analysed with a TCD.

The thermogravimetric analyses (TGA) of the samples after the catalytic reactions were performed in air using the TGA 1 Star System of Mettler Toledo. About 10 mg of sample was heated from room temperature to 100 °C, left at this temperature for 1h and then heated to 1100 °C at the rate of 10 °C/min in 30 ml/min of flowing air.

Transmission electron microscopic (HRTEM) images were collected by JEOL JEM 2100 microscope. Lacey carbon Formvar coated Cu grid was used for sample preparation

2.3 Catalytic measurements

The FTS tests were carried out in a continuous-flow quartz reactor (i.d. 12 mm) with a catalyst loading of 0.5 g. The catalyst powder (sieved fraction between 180 and 250 mm) was diluted 1:2 with inert SiC in order to avoid hot spots. Tests were performed at atmospheric pressure, using a reaction feed of CO, H_2 and He (CO:H_2:He volume ratio of 1:1.7:2.3) at 30 ml/min, with GHSV = 3600 $ml_{syngas}\ g_{cat}^{-1}\ h^{-1}$, in a temperature range 275-350 °C. The catalyst was heated to the selected temperature using a heating rate of 10 °C/min. It remained 120 min at each of the three temperatures (275 °C, 300 °C and 350 °C). During that time, 4 analyses of products and reagents were performed until stable readings were obtained. Prior to reaction, the catalysts were reduced in situ in pure H_2 flow (25 ml/min) at atmospheric pressure for 16 h at 350 °C. The product gases were analysed with a TCD and a flame ionization detector (FID). H_2, CO, CH_4 and CO_2 were separated

by a Carbosieve II packed column and analysed by the TCD. Products C_1-C_4 were separated by an alumina-plot column and quantified on the FID. The CO conversions were calculated as Xco = 100 x (mol $_{CO_{in}}$- mol $_{CO_{out}}$) / mol $_{CO_{in}}$. Selectivity to the lower hydrocarbons S_{Cx}, to CO_2 and to the oxygenates was calculated from the corresponding moles and from the converted CO as S_{Cx} = $xmol_{Cx}$ /($mol_{CO_{in}}$- $mol_{CO\ out}$) x 100. Selectivity to hydrocarbons with a number of carbon atoms ≥ 5 was obtained as $S_{C5+} = 100-(S_{C1} + S_{C2-C4} + S_{CO2})$ [23]. The conversion rate at different temperatures, reported as moles of converted CO per minute and per grams of catalyst along with selectivity values were determined after 2h reaction time. It is worth saying that the selected operational regime avoided the formation of long chain hydrocarbons (wax) usually obtained with the FTS process at elevated pressure [18].

3. Results and Discussions

3.1 Catalytic results

The catalytic results in terms of CO conversion rate and selectivity at the three different temperatures are summarized in Table 1. By comparing the conversion rates within each column, with the exception of the 300 °C data, an increase of the rate, from the monometallic iron catalyst to the cobalt containing catalysts, reaching the highest values with the 10Co2Fe/TiO_2 catalyst, is observed. It is also worth noting that whereas the monometallic iron catalyst decreased its activity at the highest temperature of 350 °C, the cobalt containing catalysts substantially increased their activity. The selectivities to different carbon compounds, such as CH_4, C_2-C_4 and C_{5+} , for the different catalysts, are also summarized in Table 1. Additionally, for clarity sake, the selectivities at the three different temperatures of 275 °C, 300 °C and 350°C are shown in the bar diagrams in Fig. 1. The diagrams contain also the CO_2 selectivity. The monometallic cobalt catalyst exhibited a 65% selectivity towards CH_4 at 275 °C and 300 °C. At the same temperatures, selectivities to C_2-C_4 and C_{5+} of the order of ~ 8 % and ~ 27 % respectively were obtained. At 350 °C methane production decreased and higher hydrocarbon selectivity increased, in accord with what reported in literature [11]. As expected, due to the renowned iron activity in water gas shift reaction (WGSR), the monometallic iron catalyst, differently from the pure cobalt catalyst, produced large amount of CO_2 at each of the three considered temperatures [24]. Moreover, by increasing the temperature from 300 °C to 350 °C, an increase of the heavier hydrocarbon production with respect to the C_2-C_4 was observed. It is worth noting that with the monometallic iron catalyst methanol formed. These results are in accord with what recently reported on similar catalysts, using a microchannel reactor operating at 1 atm [15]. Concerning the two bimetallic systems, 6Co6Fe/TiO_2 and 10Co2Fe/TiO_2, comparable and conspicuous amounts of C_2-C_4 and C_{5+} were produced at 275 °C and 300 °C. Methane was produced to a less extent as compared to the monometallic cobalt catalyst. At 350 °C,

the methane selectivity noticeably decreased with both bimetallic catalysts in favor of increasing amount of heavier hydrocarbons (~60 %). Besides, more methanol was produced at 275 °C and 300 °C in comparison to the amount produced by the monometallic iron catalyst. The relatively low GHSV, with consequent longer bed residence time helping the re-adsorption of olefin, favored the production of C_2-C_4 and C_{5+} hydrocarbon [25]. Overall, the catalytic performance of the bimetallic CoFe catalysts, in terms of alcohol and heavier hydrocarbon selectivity appear promising when compared to other cobalt or iron system operated at atmospheric pressure and at even lower GHSV [15, 26].

In order to check for hydrocarbon products retained on the catalyst, thermogravimetric analyses (TGA) in air were performed on the samples after completion of the catalytic test, i.e. after the last temperature set of data. The TGA curves with the relative differential plots are shown in Fig. 2. All the catalysts presented a weight increase due to the oxidation of reduced species. The increase was much more evident in the monometallic catalysts for which no weight loss was registered. On the contrary, the bimetallic ones, 6Co6Fe/TiO_2 and 10Co2Fe/TiO_2 underwent weight loss equal to 8% and 10% respectively. The weight loss occurring in the temperature range of 300 °C - 420 °C corresponded to the combustion of carbonaceous compounds deposited on the catalyst during the reaction. The extent of the weight loss was related to the higher conversion rate and the larger selectivity toward heavier hydrocarbons measured for the bimetallic samples.

3.2 Characterization results

BET

The list of catalysts and support with the corresponding BET specific surface areas, pore diameters and pore volumes is given in Table 2. The N_2 adsorption - desorption isotherms along with the pore sizes distribution are shown in Fig. 3. According to the IUPAC classification, the isotherms are of type IV, characteristics of mesoporous materials, with clear hysteresis loops of H1 type [27]. The addition of the cobalt and /or iron did not modify significantly the textural properties in terms of specific surface area and pore sizes of the initial TiO_2.

TPR

Reducibility of the catalysts was investigated by performing TPR analyses. The TPR profiles of the calcined samples are shown in Fig. 4. The profile of the monometallic cobalt sample exhibited a main peak at 347 °C with a shoulder at around 290 °C, attributable to reduction of Co_3O_4 to CoO and a broad peak centred at about 500 °C due to the reduction of CoO to Co [25]. At variance with what reported in literature for TiO_2 supported cobalt catalysts, these reduction temperatures were quite low and reflected the presence of large Co_3O_4 particles not strongly

interacting with the TiO_2 support [14, 28-29]. The profile of the monometallic iron catalyst was characterised by two main peaks, one, narrow and small, at 347 °C due to reduction of Fe_2O_3 to Fe_3O_4 and another one, quite big, centred at 590 °C, attributable to the reduction of Fe_3O_4 to FeO. The broad feature peaked at around 960 °C could be attributed to the reduction of Fe(II) strongly interacting with the TiO_2 support. With the exception of this feature, the profile resembled very much the profile of a bulk Fe_2O_3 sample [15, 25]. The profile of the bimetallic 6Co6Fe/TiO_2 was characterised by a main peak at 435 °C, at a temperature value in between the temperatures of the main reduction peaks of the monometallic samples. The profile of the cobalt enriched catalyst presented a large peak at 484 °C and a small peak at 290 °C. In accord with what reported in literature, the profiles of both bimetallic catalysts arose from a chemical interaction between the two oxides, with cobalt increasing the reducibility of the iron oxide and the iron playing an opposite effect on the cobalt oxide [13, 25]. The hydrogen uptake was lower than what expected on the basis of the chemical composition. Such discrepancy was in accord with the theory of the strong metal support interaction effect (SMSI) reported for a support like TiO_2 and determining a metal particle decoration by the support itself inhibiting the hydrogen adsorption [30]. The effect was more pronounced with cobalt, suggesting that beside the SMSI, some unreducible oxide such as a mixed cobalt titanate could have been formed [28].

XRD

X-ray diffraction patterns of the monometallic catalysts and bimetallic 6Co6Fe/TiO_2 as fresh and as spent samples are shown in Fig. 5. All patterns exhibit reflections due to the anatase and rutile phases of TiO_2. The weight fraction of the rutile phase (W_R) in the pure support and in the catalysts was calculated according to the following formula:

$$W_R = 1/[1+0.884\ (A_{anatase}/A_{rutile})]$$

where $A_{anatase}$ and A_{rutile} represent the X-ray integrated intensities of the most intense diffraction peaks anatase (101) and rutile (110) [14, 31]. As reported in Table 2, the support alone was formed mainly by anatase, with a rutile fraction around 8 %. The presence of a certain amount of rutile crystalline phase, even to this extent, according to literature, would be beneficial for the FTS catalytic activity of the supported catalysts, particularly with respect to the C_{5+} selectivity [14]. With the exception of the monometallic iron catalyst, the addition of cobalt and iron oxides contributed to a slight increase of the rutile fraction. Such structural modification of the TiO_2, might be attributed to a thermal effect caused by the supplementary calcination associated with the metal deposition procedure. After the FTS reaction, the rutile fraction slightly decreased. The corresponding crystallite sizes of the anatase and rutile, as obtained from Sherrer equation, are also listed in Table 2 for the fresh and for the spent samples. It is worth noting the diminished sizes in the aged samples of both anatase and rutile crystallites. Such variations, i.e,, the decrease of the

rutile fraction with corresponding decrease of crystallite sizes, was indicative of a restructuring of the materials occurring during the FTS catalytic test including the H_2 pre-treatment. By looking at the diffractograms of the fresh 12Co/TiO_2 of Fig. 5, besides the TiO_2 support reflections, the characteristic peaks of Co_3O_4 are discernible (PDF; 078-1969). Through the Sherrer analysis, sizes of 38 nm were estimated for the Co_3O_4 crystallites. The corresponding pattern of the aged sample, following the catalytic reaction, exhibited peaks at 2θ = 44.6° and 41.5°. After careful examination of ICDD data base, the two peaks were attributed to a titanium cobalt alloy of composition close to $TiCo_2$ (PDF: 081-4920) [32]. The shoulder at 2θ = 44.2° was likely due to metallic Co (fcc, PDF:015-006). The diffraction pattern of the calcined monometallic iron catalyst contained, besides the support peaks, the characteristic diffraction peaks of hematite α -Fe_2O_3 phase (rombohedral , e.g. PDF:09-0599). As obtained from the Sherrer analyses the crystallite sizes were ~ 28 nm. After FT reaction the hematite peaks disappeared. The XRD pattern of the calcined 6Co6Fe/TiO_2 sample contained only the support diffraction peaks with no reflections attributable to the active elements, suggesting a good dispersion of the supported oxides. This finding was different from bimetallic cobalt and iron catalysts supported on γ- alumina, where individual Co_3O_4 and Fe_2O_3 phases were detected [25]. A stronger interaction between cobalt and iron with the TiO_2 support and also a reciprocal interaction effect, likely achieved during the catalyst preparation procedure, could have been responsible for a better dispersion of the two metals [14]. Indeed, the presence of a cobalt titaniun alloy, registered in the monometallic catalyst after FTS, would confirm such hypothesis. The peaks at 44. 9° 2θ and at 65.4° 2θ present in the pattern of the 6Co6Fe/TiO_2 aged sample were attributed to an alloy CoFe (PDF: 049-1568) with composition close to the analytical molar ratio Co/Fe = 1. The XRD patterns of the bimetallic 10Co2Fe/TiO_2, as calcined, reduced and aged sample, are shown in Fig. 6. Contrary to what observed for the catalyst with equal loading of cobalt and iron, Co_3O_4 diffraction peaks were present in the XRD pattern of the calcined sample with corresponding estimated crystallite sizes of 14 nm. The presence of iron had definitely limited the cobalt oxide particle growth during the calcination of the catalyst. Upon reduction at 350 °C, the XRD pattern contained a peak at 44.2° 2θ attributed to metallic cobalt (PDF: 015-006) and a peak at 45.1° 2θ attributed to a cobalt enriched $Co_{0.7}Fe_{0.3}$ alloy (PDF:048-1818). Particle sizes of 17 nm for both, Co and alloy, were obtained. After reaction, the pattern remains unchanged, except for a narrowing of the two above mentioned peaks, due to sintering, with an increase of the crystallite sizes up to 25 nm and 21 nm for Co and $Co_{0.7}Fe_{0.3}$ respectively. To further investigate the formation of cobalt –iron alloy in correspondence of a different loaded Co/Fe atomic ratio, the XRD analysis of the 6Co6Fe/TiO_2 after H_2 treatment was also performed. For comparison purpose, in the inset of Fig. 6 a close up of the Co_xFe_y alloy angle region of pre-reduced 6Co6Fe/TiO_2 and 10Co2Fe/TiO_2 is shown. Clearly, the pattern of the former sample does not contain any pure metallic cobalt peak,

but only peak attributable to the CoFe alloy with composition 1:1 (PDF:049-1567) and an estimated crystallite size of 21 nm which, after reaction, did not change. Such additional result confirmed that the alloy was formed during the H_2 reduction treatment and remained during the FTS reaction. To summarize, when cobalt and iron were together in a 50/50 amount, upon calcination, Co_3O_4 did not crystallize or was highly dispersed, likely due to a reciprocal effect played by the two metal oxides. Upon reduction, the catalyst gave rise to CoFe alloy. In the case of the cobalt enriched catalyst, XRD detectable Co_3O_4 formed upon calcination. Then, during reduction, it transformed into a cobalt enriched $Co_{0.7}Fe_{0.3}$ alloy and metallic Co. Such phases remained even after catalytic reactions. It is worth noting that the alloy crystallites in both cases sintered to a less extent as compared to the metallic Co. To the best of our knowledge no clear evidence of CoFe alloys have been so far reported in relation to FTS catalytic reactions. Moreover, it is interesting to notice that, as it was speculated some time ago for bimetallic CoFe systems [16] but contrary to what recently reported in the literature, under the present experimental condition, no evidence for metal carbide formation in neither monometallic and bimetallic catalysts was found [15,18].

HRTEM

In Fig.7 the HRTEM images of the 10Co2Fe/TiO_2 and 6Co6Fe/TiO_2 catalysts, respectively first and second row of images, as fresh oxides and after the FTS test, with the lattice distances marked in red, are shown. The lattice fringes of ca. 0.25 nm and 0.29 nm, visible in the panel a) referring to the calcined 10Co2Fe/TiO_2 sample, were attributed to the (311) and (220) facets of Co_3O_4 [33]. In the image b) referring to the sample after the catalytic reaction, the interplanar spacings of 0.47 nm and 0.26 nm were attributed to a defective titania like Ti_3O_5. In other parts of the same sample lattice fringes of 0.36 nm typical of anatase TiO_2 were also present. For the calcined 6Fe6Co/TiO_2, the image in panel c) has marked lattice spacing of 0.49 nm and 0.26 nm attributed again to defective titania and a spacing of 0.25 nm typical of Co_3O_4 crystallites. On the bases of similar lattice spacing, attribution to particles of α-Fe_2O_3 could not be excluded. However, the amount of either oxide crystallites must be rather spare since, as discussed above, no reflections due to hematite or cobalt spinel were detected in the XRD pattern of this sample. The image in panel d) referring to the sample after catalytic reaction contains particles with spacing of 0.20 nm, attributed to the CoFe crystallites, in accord with the XRD finding. Fringes at 0.36 nm and 0.49 nm due to anatase TiO_2 and to defective Ti_3O_5 were also present in other parts of the sample, not shown in here. It is worth to note that, over the samples analyzed after catalytic reaction, the HRTEM images did not evidence any graphitic carbon or metal carbide species in accord with the XRD results, whereas they reveal a consistent de-structuring of both samples.

XPS

In order to investigate the surface of the catalysts, X-ray photoelectron spectroscopy analyses were performed. In Table 3 the XPS results obtained from the calcined and aged samples are summarized in terms of the principal catalyst binding energies and atomic ratios. For all the analyzed samples, the Co $2p_{3/2}$ spin orbit component of the calcined samples contained two contributions attributed to two chemical species, Co^{2+} and Co^{3+}. The Co^{2+} was characterized by the Co $2p_{3/2}$ spin orbit component at a binding energy of 781.2 ± 0.2eV with a related shake up peak about 5 eV towards higher energy. The Co^{3+} species was characterized by Co $2p_{3/2}$ component at 779.8 ± 0.2 eV. The presence of the two chemical components was in accord with surface Co_3O_4 although the XPS derived Co^{3+}/Co^{2+} atomic ratio was lower as compared to the stoichiometric 2:1 ratio [12, 34]. After catalytic reaction, a component at lower binding energy, 778.1 eV, typical of metallic cobalt, was present. The Co 2p spectra for the selected sample 6Co6Fe/TiO_2 are given in Fig. 8 showing also the spectrum of the sample after the H_2 treatment at the same pretreatment conditions prior the catalytic test. The spectrum of the reduced sample exhibited the component at 778.1 eV typical of metallic cobalt. Moving to the iron XPS results, as seen in Table 3, all the iron containing samples had the Fe $2p_{3/2}$ spin orbit component characterized by two peaks, a more intense peak at 710.3 ± 0.1eV typical of Fe^{2+}, accompanied by a small satellite at 8 eV towards high energy and a smaller one at 712.5 ± 0.1 eV eV, due to Fe^{3+}. The Fe 2p spectra of the sample 6Co6Fe/TiO_2 at different moment of the catalyst life are shown in Fig. 9. The calcined sample was characterized by Fe 2p spectrum exhibiting the two components, Fe^{2+} and Fe^{3+} [35]. However, as shown in the spectra of Fig. 9 the relative ratio of the two species Fe^{3+}/Fe^{2+} was not in the stoichiometric amount of 2:1, typical of the Fe_3O_4 phase but reflected a surface enriched in Fe^{2+} [35]. After the hydrogen treatment, at the same conditions prior the catalytic test, the presence of an additional Fe $2p_{3/2}$ peak at 707.5 eV with the corresponding Fe $2p_{1/2}$ at 718.6 eV indicated formation of metallic iron. After the catalytic test, the signal deteriorated and the metal component disappeared. Moreover, according to the XPS results of the reduced catalyst, only low percentages of metallic cobalt and metallic iron were observed. This result was in accord with the TPR profile, which for the particular case of 6Co6Fe/TiO_2 sample, revealed a complete reduction of the sample at about 580 °C. With respect to the XPS derived surface atomic ratios listed in Table 3, it is worth noticing the decrease of the Co/Ti ratio and at the same time a decrease of the Fe/Co ratio in the bimetallic samples, going from the fresh to the spent catalysts. Both findings were in agreement with TiO_2 diffusing to the surface, because of a strong metal-support interaction, and with a surface segregation of cobalt with respect to iron, after the catalytic test. The C1s XPS spectra, not reported here, provided additional information on the carbon species deposited in the spent catalysts. In accord with the TGA results, only the bimetallic samples exhibited a significant increase of the C 1s peak intensity at 284.8 eV, slightly shifted with respect to the adventitious hydrocarbon set at 285.1

eV. The binding energy of this carbon peak could correspond to amorphous or graphitic carbon species [36].

According to the characterization data, the adopted preparation procedure likely had favored the formation of CoxFey alloys during the H_2-treatment prior the catalytic test. These crystallites had a positive influence on the catalytic activity of the cobalt –iron system in FTS reaction. The intimate contact between the two active metals has determined catalytic sites with electronic and morphological properties suitable for the chain initiation and chain propagation process during the FTS reaction. Moreover, the intimate contact between the two metals, but also between the metals and the $TiO2$ support avoided sintering of the active sites during the time of the catalytic test and also prevented the formation of inactive carbides.

4. Conclusion

The present study has demonstrated the feasibility of ambient pressure FTS process using cobalt-iron catalyst supported on TiO_2. The test conducted with a H_2/CO ratio below the stoichiometric value of two has produced methane, especially with the monometallic cobalt, but also significant amount of C_2-C_4 and higher C_{5+} hydrocarbons. The best performance in terms of CO conversion rate and selectivity was exhibited by the formulation $10Co2Fe/TiO_2$. Quite interesting and not so far explicitly reported in literature for similar type of catalysts, Co_xFe_y alloys with composition depending on the analytical loading of the two elements were formed during the pre-reduction treatment. It was rather peculiar that the alloy formed in the presence of a very interacting support like TiO_2, therefore overcoming the tendency to give hardly reducible titanate. The adopted procedure for the catalyst preparation, involving the use of the microwave, as observed in previous work, favored a strong interaction between the two metal oxides. Such interaction was preserved during reduction and also during the catalytic test, avoiding the formation of metal carbides which, especially for the cobalt, are known to lead to the catalyst deactivation. In consideration of these preliminary results, further investigations are needed to ascertain the role of a Co_xFe_y alloy into the mechanism of the FTS reaction.

Acknowledgments

The Executive Programme for Cooperation between Italy and India (Prot. No. MAE01054762017) is kindly acknowledged. M.R thanks P.O. FSE 2014/2020 for post graduate scholarship. F.Giordano and N.G. Gallì for their assistance with characterization techniques are kindly acknowledged.

Table 1. Catalytic performance for the Fisher -Tropsch synthesis, at three different temperatures and 1 bar, of various catalysts, determined after 2 hours of time - on-stream at each temperature.

	$12Fe/TiO_2$ (°C)			$12Co/TiO_2$ (°C)			$6Co6Fe/TiO_2$ (°C)			$10Co2Fe/TiO_2$ (°C)		
	250	*300*	*350*	*250*	*300*	*350*	*250*	*300*	*350*	*250*	*300*	*350*
Conv rate*	1.8	2.4	1.4	2.4	2.5	3.0	2.2	1.9	15	4.5	2.0	26
Sel_{CH4}	20.6	23.8	18.5	64.3	65.8	35.8	23.8	25.7	4.8	28.1	41.6	9.1
Sel_{C2-C5}	35.0	30.9	11.1	6.9	8.9	9.8	26.9	24.8	3.1	31.1	32.3	3.8
Sel_{C5+}	13.4	9.1	35.9	28.8	24.3	54.4	19.2	12.2	62	27.1	7.6	60.8
Sel_{CH3OH}	1.0	1.5	0.9	0	0	0	5.1	6.0	0.5	5.5	6.6	0.4

*$10^{-5} mol_{CO}/gcat/min$

Table 2. BET surface area (S_{BET}), pore diameter, d_p and pore volume, V_p, of support and calcined catalysts. The metal oxide particle sizes d, the rutile weight fraction, W_R, and the TiO_2 crystallite sizes, d(nm), as determined by XRD, are also listed for the different samples.

Sample	S_{BET} (m^2g^{-1})	d_p(Å)	V_p (cm^3g^{-1})	d_{Co3O4}[a] (nm)	W_R[c]	d_{TiO2}(nm)[c]	
						Anatase	Rutile
TiO_2	27	9	0.084		8	25	55
$12Fe/TiO_2$	26	14	0.125	28[b]	8(7)	46(30)	87(49)
$12Co/TiO_2$	24	11	0.085	38	9(8)	46(32)	100(73)
$6Fe6Co/TiO_2$	29	13	0.126	n.d.	10(8)	42(29)[d](37)	79(45)[d](63)
$10Co2Fe/TiO_2$	25	14	0.090	14	9(8)	35(33)[d](34)	67(63)[d] (63)

[a] determined from the (400) and (220) and (511) reflections of the cubic Co_3O_4.

[b] d_{Fe2O3}determined from the (104) and (024) reflections of the α-Fe_2O_3.

[c] the values in parentheses refer to the samples after FTS reaction.

[d] after H_2 treatment.

Table 3. Binding Energies (eV) and Atomic ratios of the catalysts as calcined and after catalytic test.

Sample	Co $2p_{3/2}$		Fe $2p_{2/3}$		Co/Ti		Fe/Co	
	calc	*spent*	*calc*	*spent*	*calc*	*spent*	*calc*	*spent*
$12Co/TiO_2$	779.9 781.1	778.1 781.0			0.8	0.4		
$6Co6Fe/TiO_2$	779.6 781.4	778.1 780.7	710.2 712.4	710.4 712.4	0.4	0.3	0.8	0.6
$12Co2Fe/TiO_2$	779.9 781.0	778.4 781.1	710.3 712.4	710.6 712.5	1.0	0.4	0.3	0.2
$12Fe/TiO_2$			710.4 712.4	710.4 712.4	Fe/Ti calc.	spent		
					0.3	0.2		

Reference list

1) M. Höök, X.Tang, Depletion of fossil fuels and anthropogenic climate change—A review, Energy Policy 52, (2013) 797-809.
2) S. Shafiee, E.Topal, When will fossil fuel reserves be diminished?, Energy Policy 37 (2009) 181–189.
3) E. Iglesia, Design, synthesis and use of cobalt –based Fisher-Tropsch synthesis catalysts Appl. Catal. A, 161 (1997) 59- 78.
4) H. Jahangirl, J. Bennett, P. Mahjoubi, K. Wilson, S. Gu, A review of advanced catalyst development for Fisher-Tropsch synthesis of hydrocarbon from biomass derived syn-gas, Catal. Sci. Technol. 4 (2014) 2210.
5) R. Hakawati, B. Smyth, H. Daly, bG. McCullough, D. Rooney, Is the Fisher-Tropsch Conversion of Biogas-Derived Syngas to liquid Fuel Feasible at Atmospheric Pressure?. Energies 12 (2019) 1-28.
6) D. Verloet, F. Kapteijn, J. Nijenhuis, J. R. van Ommen, Fisher-Tropsch reaction-diffusion in a cobalt catalyst particle: aspects of activity and selectivity for a variable chain growth probability, Catal. Sci. Technol. 2 (2012) 1221-1233.
7) V. R. Calderone, N. R. Shiju, D. C. Derré, G. Rothenberg, Bimetallic catalysts for the Fisher Tropsch reaction, Green Chem. 13 (2011) 1950-1959.
8) M. A. Sainna, A. Mk, Catalyst and Catalysis for Fisher- Tropsch Synthesis: A comparative Analysis of Iron and Cobalt Catalysts on SBA-15, J. Thermodyn. Catal. 7 (2016) 1-8.
9) J. Gorimbo, X. Lu, X. Liu, Y. Yao, D. Hildebrandt, D. Glasser, Low-pressure Fischer-Tropsch Synthesis: In Situ Oxidative Regeneration of Iron Catalysts, Ind. Eng. Chem. Res. 56 (2017) 4267-4274.
10) S. Shetty, R. A. van Santen, Catal. Today, Co dissociation on Ru and Co surfaces: The initial step in the Fischer- Tropsch synthesis, 171 (2011) 168-172.
11) B. H. Davis, Fisher-Tropsch Synthesis: Comparison of Performances of iron and Cobalt catalysts, Ind.Eng. Chem. Res. 46 (2007) 8938-8945.
12) A. M. Venezia, V. La Parola, L.F. Liotta, G. Pantaleo, M. Lualdi, M.Boutonnet, S. Jaras, Co/SiO_2 catalysts for Fisher-Tropsch synthesis; effect of Co loading and support modification by TiO_2, Catal Today, 197 (2012) 18-23.
13) D. J. Duvenhage, N. J. Coville, Fe:Co/Tio2 bimetallic catalysts for the Fisher-Tropsch recation, Appl. Catal A 153 (1997) 43-67.
14) K. Shimura, T. Miyazawa, T. Hanaoka, S. Hirata, Fisher –Tropsch synthesis over TiO_2 supported cobalt catalyst: Effect of TiO_2 Crystal phase and metal ion loading Appl. Catal. A 460-461 (2013) 8-14.
15) R. Y. Abrokwak, M. M. Rahma, Vishwanath G. Deshmane, Effect of Titania support on Fischer Tropsch synthesis using cobalt, iron and ruthenium catalysts in silicon-microchannel microreactor, Mol. Catal. 478 (2019) 110566.
16) H. Arai, K. Mitsuishi, T. Seiyama, TiO_2-supported Fe-Co, Co-Ni and Ni-Fe Alloy catalysts for Fisher-Tropsch synthesis, Chem. Lett. 13 (1984) 1291-1294.
17) J. Hu, F. Yu, Y. Lu, Application of Fisher- Tropsch synthesis in biomass to liquid conversion, Catalysts 2 (2012) 303-326.
18) R. Warringham, A. L. Davidson, P. B. Webb, R. P. Tooze, R. A. Ewings, S. F. Parker, D. Lennon, Examining the temporal behavior of the hydrocarbonaceous overlayer on an iron based Fischer-Tropsch catalyst, RSC Adv. 9 (2019) 2609-2617.
19) D. P. Serrano, G. Calleja, R. Sanza, P. Pizzarro, Preparation of bimodal micro-mesoporous TiO_2 with tailored crystalline properties, Chem Commun.(2004) 1000-1001.
20) V. La Parola, G.Pantaleo, F. Deganello, R. Bal, A. M. Venezia, Plain and CeO_2 – Supported LaxNiOy catalysts for partial oxidation of CH_4, Catal. Today, 307 (2018) 189-196.
21) Inorganic Crystal Structure Database (ICSD). Karlruhe, Germany, 2014.

22) H.P. Klug, L.E. Alexander, X-ray Diffraction procedures for polycrystalline and Amorphous Materials, 2nd ed. John Wiley and Sons: new York, NY, USA 1974.
23) P. Munnik,P. E. de, Jongh, K.P. de Jong, Control and Impact of the Nanoscale Distribution of Supported Cobalt Particles Used in Fisher –Tropsch Catalysis, J. Am. Chem. Soc. 136 (2014) 7333-7340.
24) W. D. Shafer, M. K. Gnanamani, U. M. Graham, J. Yang, C. M. Masuku, G. Jacobs, B. H.Davis, Fisher-Tropsch: Product Selectivity-The Fingerprint of Synthetic Fuels, Catalysts, 2019, 9, 259,
25) S. Lögdberg, D. Tristantini, Ø. Borg, L.Ilver, B. Gevert, S. Järas, E.A. Blekkan, A. Holmen,Hydrocarbon production via Fischer-Tropsch synthesis from H_2-poor syngas over different Fe-Co/γ-Al_2O_3 bimetallic catalysts. Appl. Catal. B 89 (2009) 167-182.
26) B.T. Ermagamber, N. U. Nurgaliyev, L. D. Abylgazina, B. K. Kasenov, J. M. Kasenova, Fisher –Tropsch Synthesis using Cobalt Catalyst Containing Modified Shungite, Solid Fuel Chemistry, 51 (2017) 101-106.
27) M.Thommes,. K. Kaneko, A. V. Neimark, J. P. Olivier, F. Rodriguez-Reinoso, J. Rouqueroi, K. S. w. Sing, "Physisorption of Gases, with Special Reference to the Evaluation of Surface Area and Pore Size Distribution (IUPAC Technical Report)." *Pure and Applied Chemistry* 87 (9–10): 1051–69.
28) T. O. Escherman, J. H. Bitter, K. P. de Jong, Effects of loading and synthesis method of titania-supported cobalt catalysts for Fisher-Tropsch Synthesis, Catal. Today, 228 (2014) 89-95.
29) R. Riva, H. Miessner, R. Vitali, G. Del Piero, Metal-Support Interaction in Co/SiO_2 and Co/TiO_2 Appl. Catal. A 196 (2000) 111-123.
30) S. J. Tauster, S. C. Fung, R.L. Garten, Strong metal-Support Interaction. Group 8 Noble Metal Supported on TiO_2, J. Am. Chem. Soc. 1978, 100 (1), 170−175.
31) A. A. Gribb, J. F. Banfield, Particle size effects on transformation kinetics and phase stability in nanocrystalline TiO2, Am. Mineral. 82 (1997) 717-728.
32) B. B. Strauma, A. Korneva, A. R. Kilmametov, L. Lityinska-Dobrzynska, A. S. Gornakova, R. Chulist, M. I. Karpov, P. Zieba, Strucutral and Mechanical Properties of Ti-Co Alloys Treated by High Pressure Torsion, 12 (2019) 426 (1-11).
33) R. Wei, M. Fang, G.Dong,.C.Lan,.L. Shu, H. Zhang, X. Bu, J. C. Ho, High-Index Faceted Porous Co_3O_4 Nanosheets with Oxygen Vacancies for Highly Efficient Water Oxidation, ACS, Appl. Mater. Interfaces, 10, (2018) 7079−7086
34) F. Morales, F. M.F. de Groot, O. L.J. Gijzeman, A. Mens, O. Stephan, B. M. Weckhuysen, Mn promotion effects in Co/TiO2 Fischer-Tropsch catalysts as investigated by XPS and STEM-EELS, J. Catal. 230 (2005) 301-308.
35) T. Yamashita, P. Hayes, Analysis of XPS spectra of Fe^{2+} and Fe^{3+} ions in oxide materials, Appl. Surf. Sci.254 (2008) 2441-2449.
36) D. Peña, A. Griboval-Constant, V. Lecocq, F. Diehl, A. Y. Khodakov, Influence of operating conditions min a continuously stirred tank reactor on the formation of carbon species on alumina supported cobalt Fisher-Tropsch catalysts, Catal. Today, 215 (2013) 43-51.

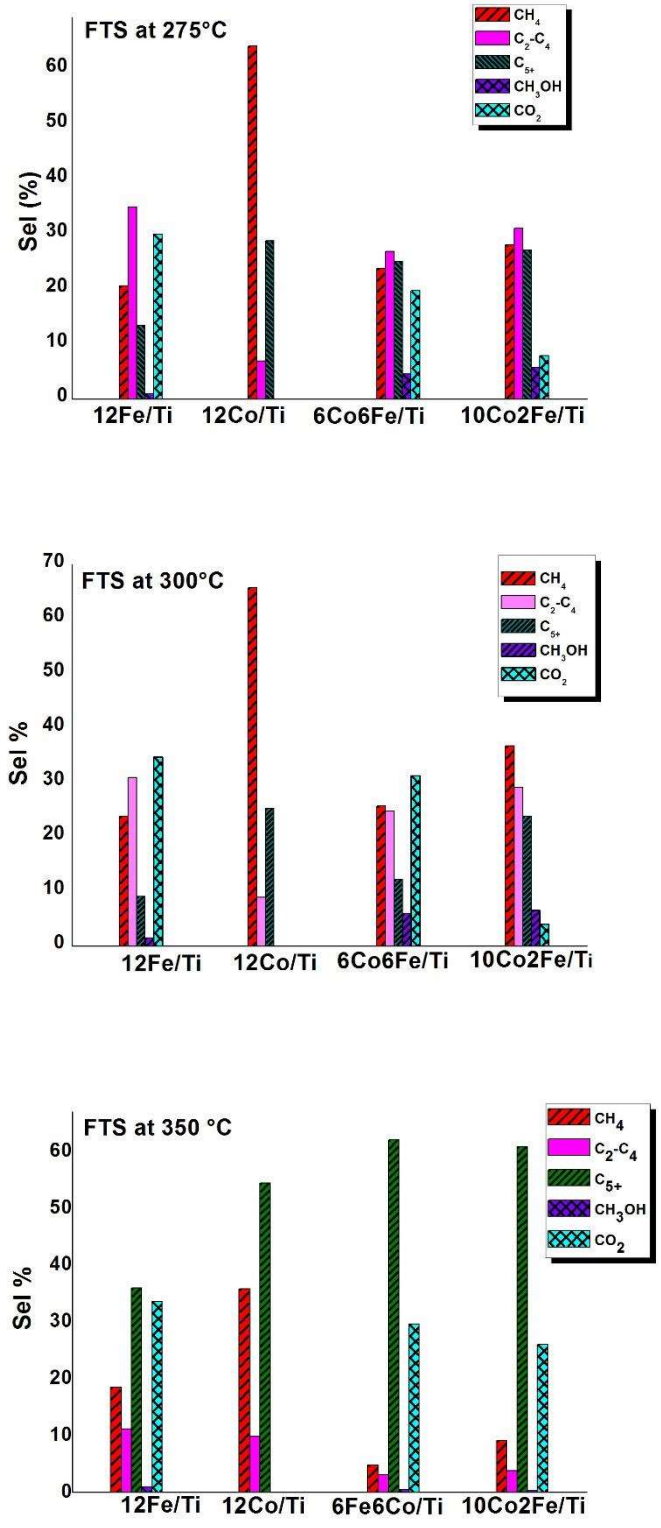

Fig. 1. FTS product selectivity over different catalysts and at different temperature. The selectivity values were calculated after 2h of time on stream.

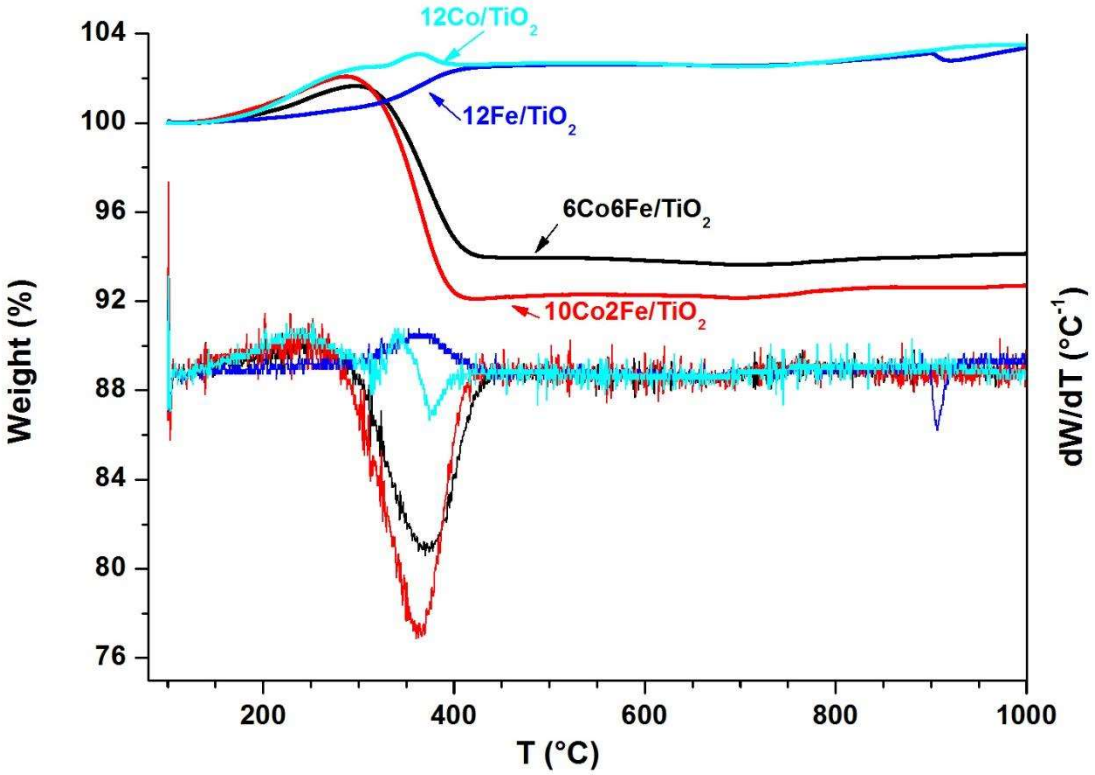

Fig. 2. TGA and DTG curves of spent catalysts.

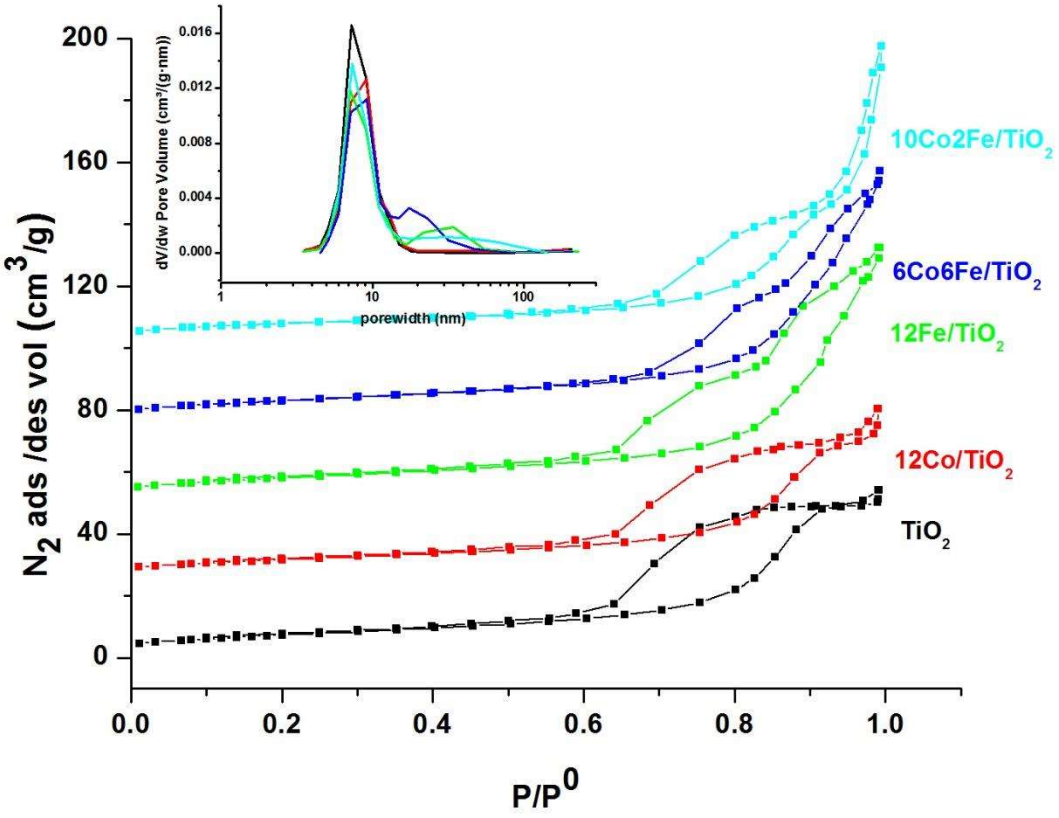

Fig. 3. N_2 adsorption/desorption isotherms and pore size distribution curves (inset) of TiO_2 supported catalysts and corresponding TiO_2 support.

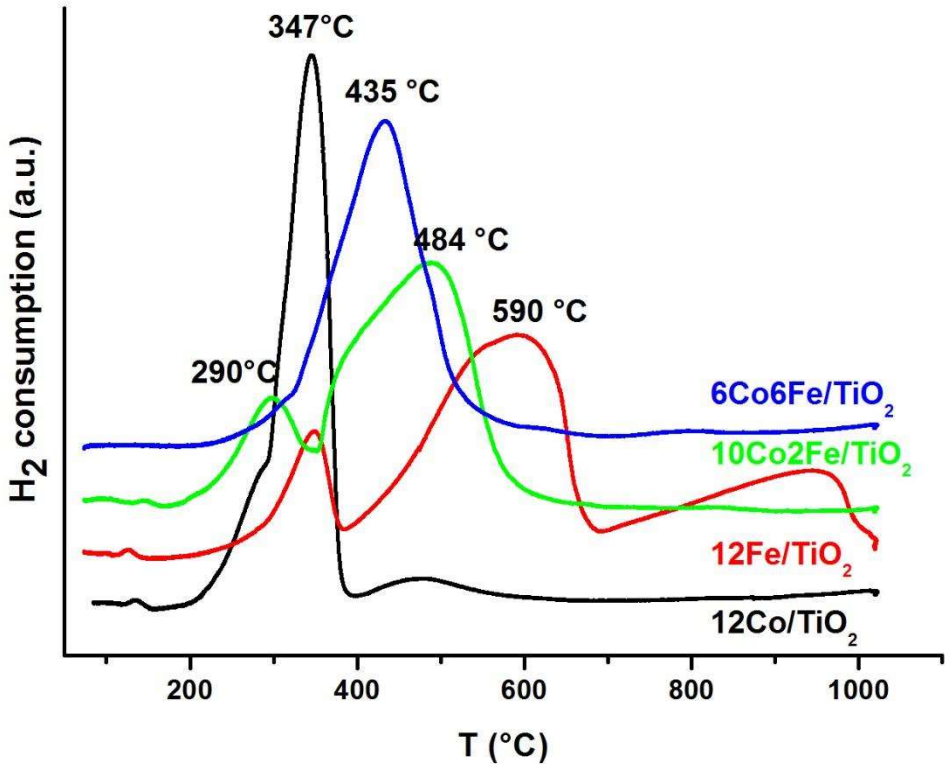

Fig. 4. TPR profiles of the TiO_2 supported catalysts.

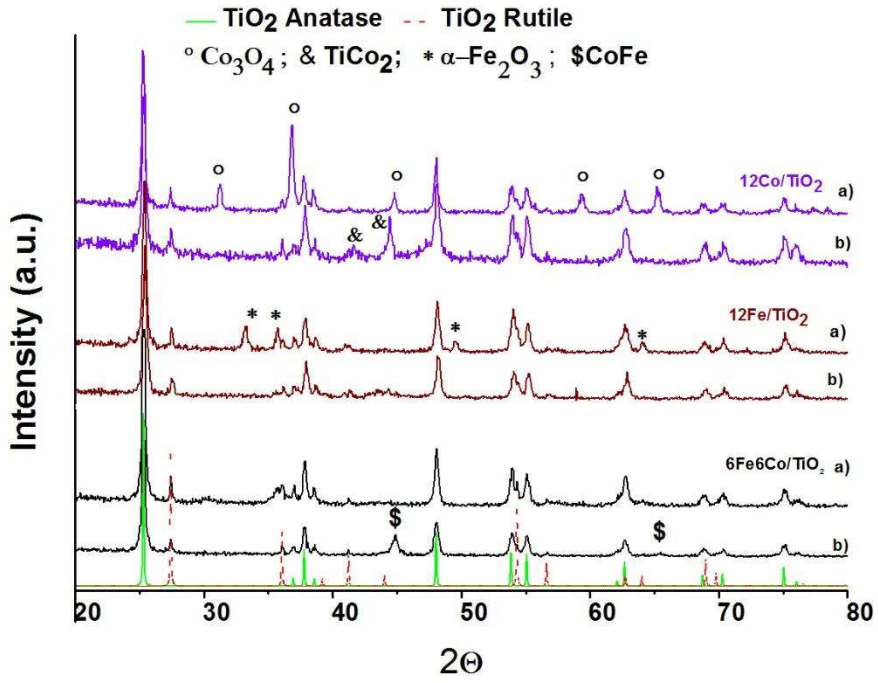

Fig. 5. Diffraction patterns of selected samples as: a) calcined; b) spent.

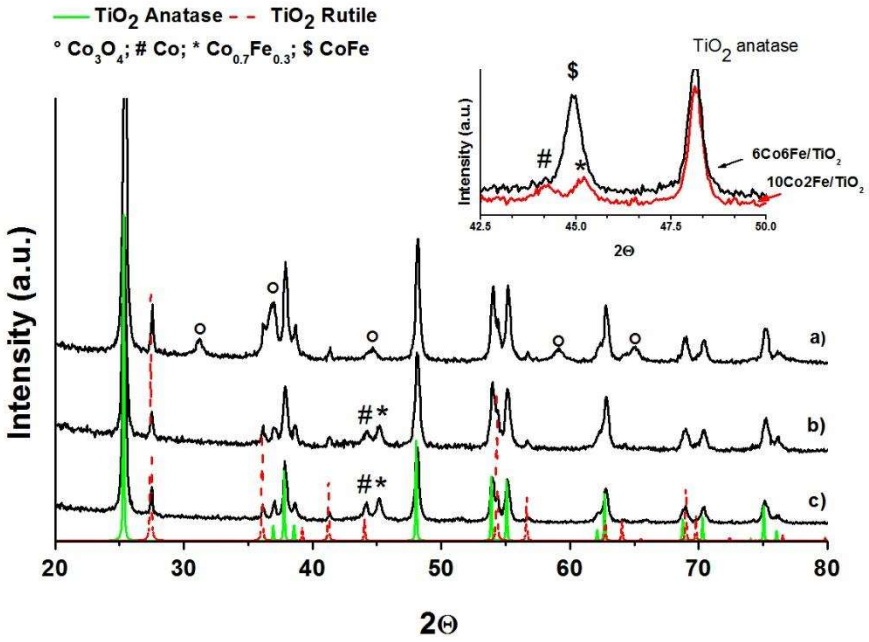

Fig. 6. Diffraction pattern of sample 10Co2Fe/TiO_2 as: a) calcined; b) reduced; c) spent. The diffraction lines of the CoFe alloy in the two bimetallic reduced catalysts are compared in the inset.

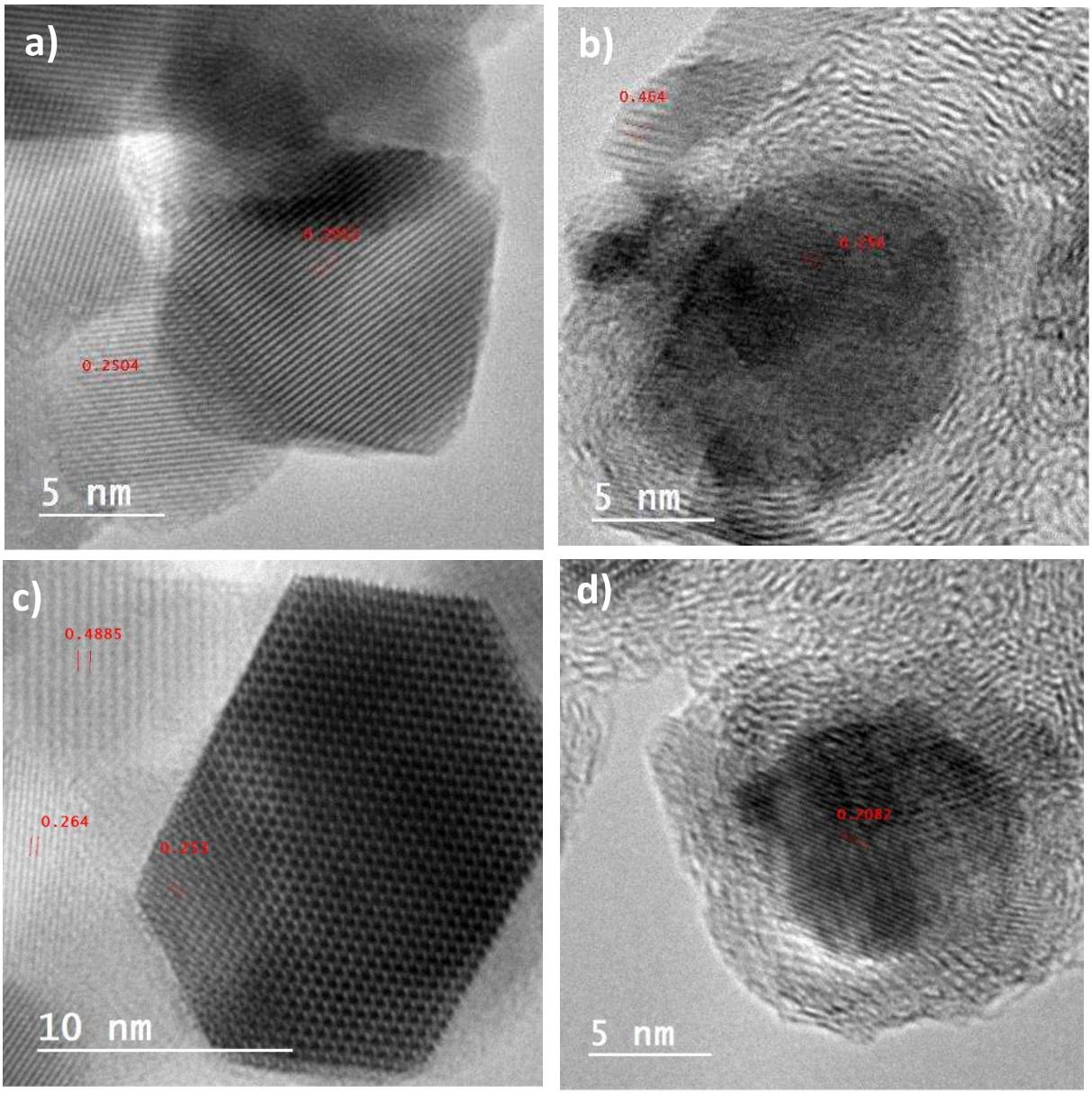

Fig. 7. HRTEM images of 10Co2Fe/TiO_2 as a) fresh catalyst; b) after FTS test. Images of 6Co6Fe/TiO_2 as c) fresh catalyst; d) after FTS test.

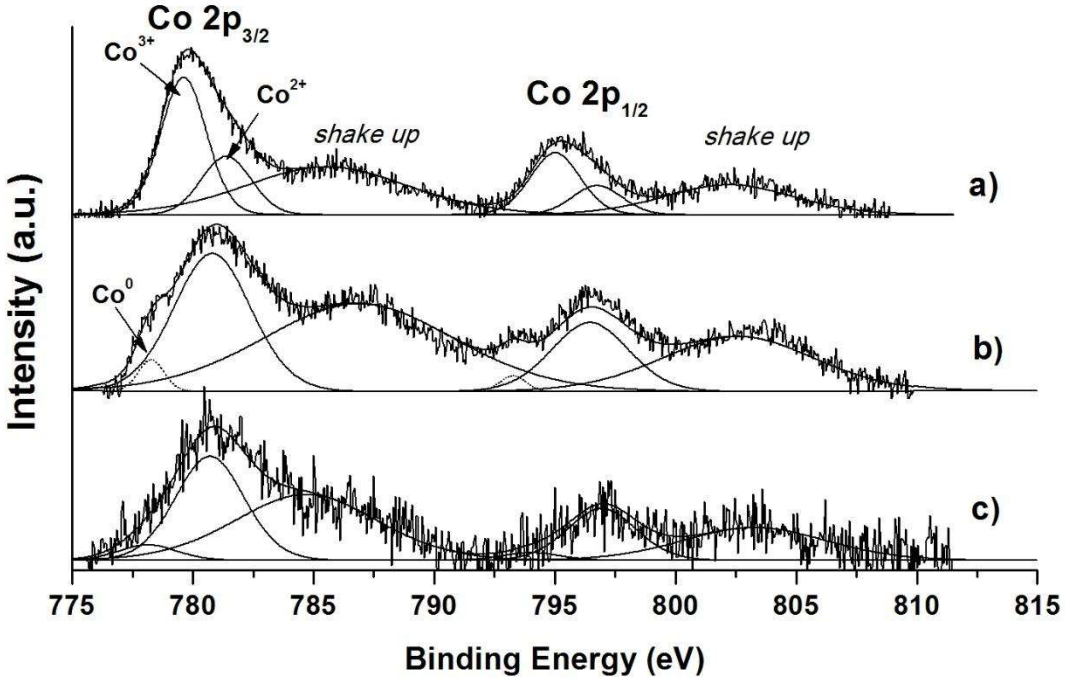
Co 2p3/2
Co3+
Co2+
shake up
Co 2p1/2
shake up
a)
Co0
b)
c)
Intensity (a.u.)
775
780
785
790
795
800
805
810
815
Binding Energy (eV)

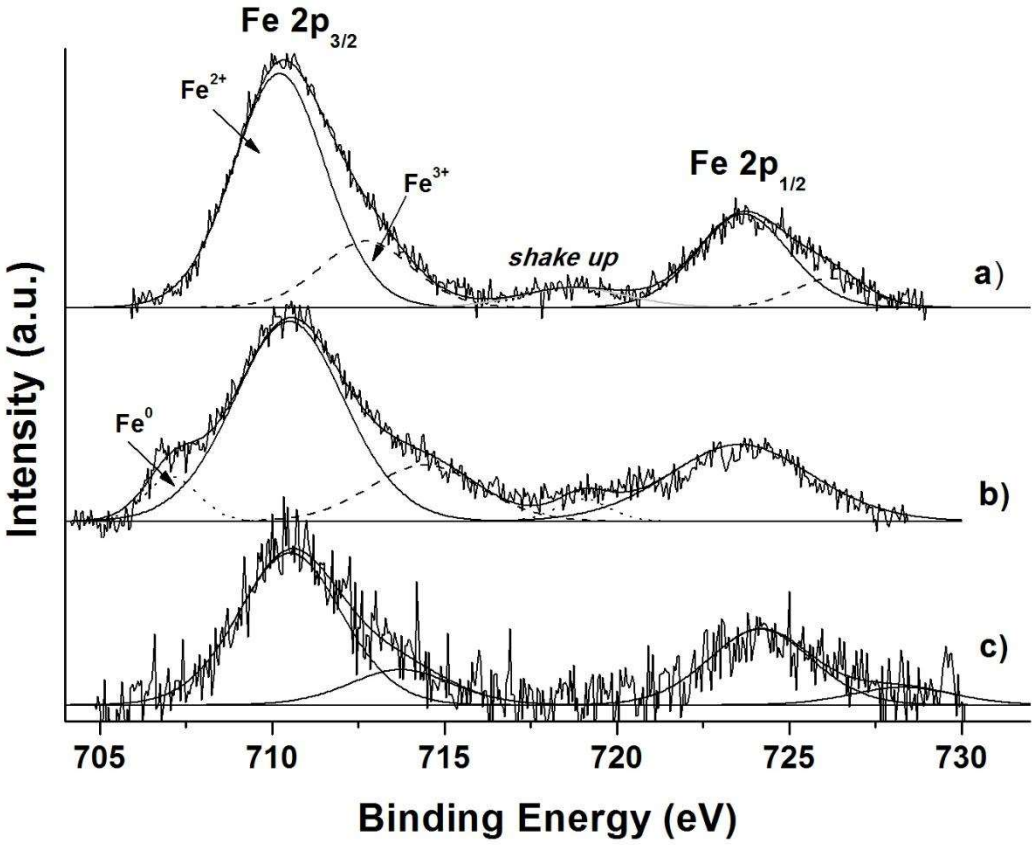

Fig. 9. Experimental and fitted Fe 2p spectra of catalyst 6Co6Fe/TiO_2 as; a) calcined; b)after H_2 reduction at 350 °C; c) after FTS reaction.